1
Chemical Reactions for the Synthesis of Organic Nanomaterials on Surfaces

Hong-Ying Gao, Oscar Díaz Arado, Harry Mönig, and Harald Fuchs

1.1
Introduction

The bottom-up growth of covalently connected organic networks is a fascinating approach for the development of new functional nanomaterials with tunable mechanical and optoelectronic properties [1–5]. Hereby, organic molecules are the building blocks, which can be deposited on a substrate by evaporation under ultrahigh vacuum (UHV) conditions or by solution growth in liquid environments. By the proper design of the precursor molecules and by controlling the parameters such as deposition rates, concentrations, and substrate temperature or irradiation, chemical reactions can be induced. This can lead to the formation of either conjugated polymers or 2D covalently connected networks [6–8]. The structural and optoelectronic properties of these products can be adjusted by the manifold possibilities of organic chemistry, which allows tailoring the reactive end groups, and the geometry as well as the electronic properties of the reactants. Following this idea, nanoscale devices ranging from simple wires to transistors, capacitors, or solar cells can be envisioned. Although recent years have shown significant progress in this field, there are only a few established on-surface reaction mechanisms that actually lead to covalent coupling directly at surfaces. Therefore, there are still considerable scientific challenges at play, making it a current hot topic in nanotechnology [2,5,6].

To study the chemical processes involved in the synthesis of such materials, experimental techniques with high lateral resolution are particularly desirable. Therefore, scanning probe microscopy and in particular scanning tunneling microscopy (STM) and noncontact atomic force microscopy (NC-AFM) have become the standard characterization tools providing direct insight into reaction mechanisms. These techniques offer topographic and electronic information of single molecules and on-surface chemical processes with high resolution [9–11], and the probe tip itself can be used to trigger chemical reactions [12–14] or to manipulate molecular species at surfaces [15,16]. Furthermore, both STM and NC-AFM experiments can be performed under different environmental

Soft Matter Nanotechnology: From Structure to Function, First Edition.
Edited by Xiaodong Chen and Harald Fuchs.

conditions, such as in UHV, in liquids, or in gaseous environments, providing further versatility to the targeted experiments. Many studies also rely on complementary experimental techniques such as X-ray photoelectron spectroscopy (XPS) or temperature-programmed desorption (TPD). From the theory side, density functional theory (DFT) is applied to describe adsorption geometries and chemical processes that take place on various substrates.

In the following, the so far established on-surface reaction mechanisms are reviewed, which potentially can be utilized for the bottom-up growth of covalently connected organic networks. Other approaches where surfaces are exclusively involved to catalyze reactions and where the products do not stay on the surface are not considered in this chapter. Besides a general overview of the various reaction types, we present a compilation of the results obtained by our group at the University of Münster, which contributed to this exciting research field.

1.1.1 Ullmann Coupling

This particular reaction is the most studied one in the recent years. It involves the thermal activation of precursor molecules with halogenated moieties after or during deposition on a substrate, which, by the supply of heat, leads to the formation of C−C bonds between the radicalized reactants. This reaction has been performed mostly on metal substrates. However, recently it has been shown to also proceed on insulators [17], which represents a significant step forward toward potential applications of the Ullmann coupling mechanism. The halogen specie mostly studied is bromine [18–24], although successful covalent coupling after scission of terminal iodine [19,25–27] and chlorine [17,28] has also been reported. The difference in activation temperature for the different carbon–halogen species has allowed to hierarchically control the formation of two-dimensional networks [19,24]. Another interesting nanomaterial with functional electronic properties developed with this method is based on graphene nanoribbons. These are obtained by a two-step reaction sequence where after initial on-surface Ullmann coupling, a further annealing step at a higher temperature leads to cyclodehydrogenation of adjacent aromatic species [23,29]. In particular, graphene nanoribbons were also successfully grown on a stepped Au(788) surface, which form well-defined (111) terraces with a width of about 3.8 nm along the [01–1] direction (Figure 1.1). This allows to gain control over the orientation of the nanoribbons, which predominantly grow along the terraces. High-resolution direct and inverse photoemission experiments of occupied and unoccupied states allowed to determine the energetic position and momentum dispersion of electronic states, which showed a bandgap of several electronvolts for different types of graphene nanoribbons [23,29].

It has been demonstrated that in general it is possible to achieve covalent bonding between organic molecules and metal atoms on surfaces [11,30].

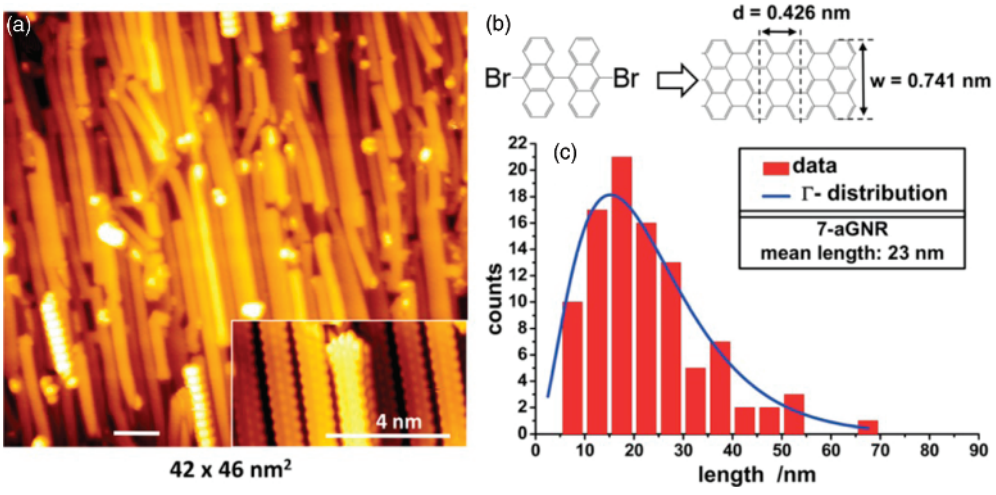

Figure 1.1 (a) STM image of spatially aligned graphene nanoribbons on a Au(788) surface. (b) After initial Ullmann coupling at a substrate temperature of 440–470 K, an additional heating step at 590 K results in a dehydrogenation process leading to the formation of the nanoribbons. (c) Statistical distribution of the ribbon length. (Reprinted figure with permission from [29]. Copyright (2012) by the American Physical Society.)

Therefore, there are also efforts to not directly bind the organic building blocks for supramolecular structures, but instead use metal atoms to mediate the coupling. Following this approach under UHV conditions, covalent bonding between tetracyanobenzene molecules and Mn atoms was accomplished to form Mn-phthalocyanine [31]. In another study, strong bonds between metal atoms and dehalogenated reactants have been shown to play an important role in the on-surface Ullmann coupling, stabilizing two-dimensional networks [24]. Furthermore, an on-surface chemical reaction between copper ions and quinone ligands at the liquid/solid interface of a Au(111) surface has been shown to successfully form two-dimensional metal–organic polymers [32].

The results on metal–organic materials lead to further developments, which use Ullmann coupling to form gold–organic hybrids, where chemical bonding between organic precursor molecules is mediated by bonding to a substrate gold atom. With this approach, the on-surface synthesis of gold–organic linear polymers by the dehalogenation of chloro-substituted perylene-3,4,9,10-tetracarboxylic acid bisimides (PBIs) was accomplished on the Au(111) and Au(100) surfaces [17,28]. Figure 1.2a shows an STM image after depositing the PBIs at room temperature on a Au(111) surface, leading to a self-assembled monolayer of the unreacted molecules. The STM contrast features a combination of two small bumps and a big rod corresponding to the short alkyl chains and the aromatic core of the PBI molecule, respectively. The bright spots on both sides of the core correspond to the twisted two chlorine atoms. Linear molecular chains were formed via depositing the precursor molecules on a 490 K preheated

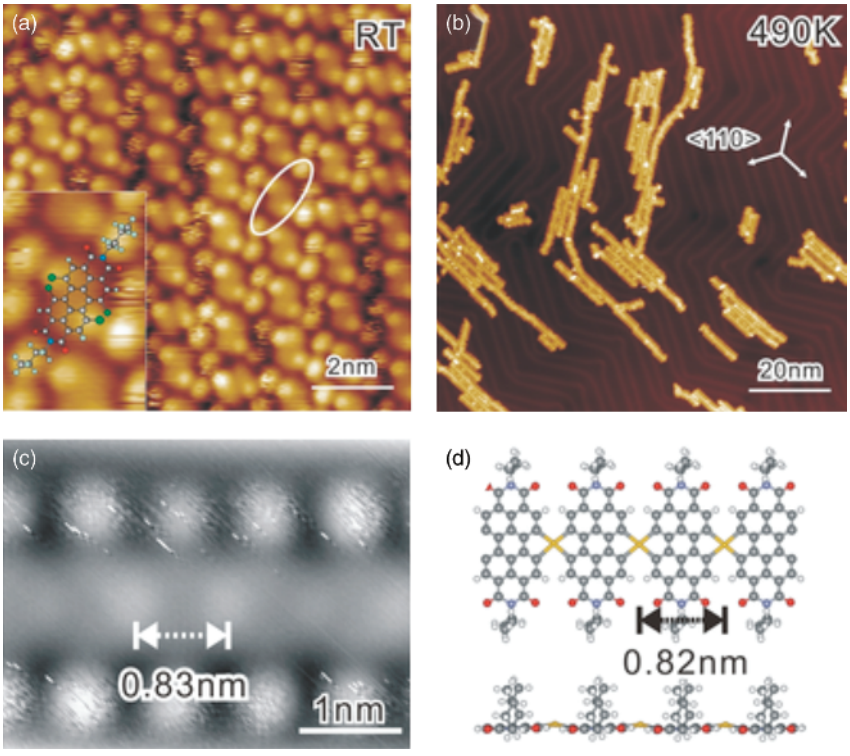

Figure 1.2 Ullmann reaction to form gold–organic hybrids. (a) The self-assembly structures of tetrachloro-PBI at a Au(111) surface (10 nm × 10 nm). (b) Polymerized molecular chains of tetrachloro-PBI on a Au(111) surface (via depositing molecules onto the hot surface of a substrate at 490 K). (c) High-resolution STM image of a polymerized PBI–Au chain and (d) its proposed chemical structure. (Reproduced with permission from Wiley-VCH Verlag GmbH [28].)

Au(111) surface at a deposition rate of about 0.1 monolayer per hour. Figure 1.2b is a representative STM image of the reaction products, in which polymers with a length of up to 70 nm can be observed. Interestingly, the orientation of the molecular chains was found mainly along ⟨110⟩ directions on the Au(111) surface. A high-resolution STM image of such a polymer is shown in Figure 1.2c, with its proposed chemical structure shown in Figure 1.2d. The measured periodic distance along the chain is (0.83 ± 0.04) nm, which matches well with the theoretical distance of 0.82 nm as determined by DFT calculations. Further experiments with the PBI deposited on the reconstructed Au(100) surface showed that on this surface the polymerization occurs exclusively along the [011] direction [28]. Further DFT calculations on a simplified model system confirmed that the reaction mechanism involves an intermediate state where a PBI radical generated from the homolytic C−Cl bond dissociation binds to a surface

gold atom, which partially is pulled out from the surface to form a stable PBI–gold hybrid species.

1.1.2 Condensation Reactions

Condensation reactions are commonly referred to as dehydration synthesis, which involves the combination of two functional groups to form a unique covalently bound product, together with a small molecular by-product, following an addition–elimination mechanism. Several condensation reactions have been proven to be suitable candidates for on-surface synthesis and have received increased attention due to their reversibility by simply adding a solution with a certain concentration of the by-product [33,34]. Successful polyimide condensation [35,36] was accomplished on a Au(111) surface by reacting anhydrides and amines with H_2O as a by-product, where the careful design of the reactants allowed to obtain both polymeric strands and porous networks. Moreover, by reacting aldehydes and amines on Au(111) [37,38], successful polyimine condensation was accomplished to produce 1D and 2D polymers on a substrate, together with H_2O as a by-product. This process has also been successfully accomplished at a liquid–solid interface on highly oriented pyrolytic graphite (HOPG) [34]. Furthermore, with HCl as a by-product, two on-surface condensation reactions have been performed to successfully form 2D porous covalent networks: polyester condensation [39] by reacting alcohols and acyl chlorides on a Au(111) surface and polyamide condensation [40] by reacting acid chlorides with amines.

However, despite the versatility of these condensation processes, the on-surface condensation of boronic acids has received most of the attention to grow nanostructures on surfaces. This chemical reaction is a good example of how noncovalent interactions controlling self-assembly processes can be used to later initiate covalent coupling between adsorbed molecules on a substrate. Furthermore, given their capability to form reversible covalent complexes, boronic acids are extensively used in organic chemistry. Taking these factors into consideration, successful on-surface covalent coupling between boronic acids has been accomplished on a large variety of substrates, such as Ag(111) [41,42], Ag(100) [41,43], Cu(111) [41], at the liquid–solid interface on HOPG [33], and Au(111) [41,44]. These studies have demonstrated not only the reversibility of the on-surface reaction, but also that the pore size and quality of the 2D networks can be tailored through careful control over the kinetic parameters of the reaction and the design of the reactants. Moreover, successful attempts to combine the success of the condensation of boronic acids and the Ullmann coupling have been carried out on Au(111) [44]. By the reaction of a single reactant charged with boronic acid and bromine moieties, subsequent stepwise activation leads to an optimization of the growth mechanism of the 2D network on that substrate, with the polymerization yield reaching almost 100%.

1.2
Alkane Polymerization

To study the on-surface polymerization of alkanes, the Au(110) surface was found to be a suitable substrate [45]. After the treatment of several sputtering–annealing cycles, this surface reconstructs to form a missing row structure along the [1–10] direction. Acting as one-dimensional constraint, the reconstruction of the surface efficiently confines the diffusion of adsorbed molecules in the [1–10] direction within the atomic channels. In the first step, *n*-dotriacontane ($C_{32}H_{66}$) was used as a precursor molecule, which was deposited under UHV conditions onto the gold substrate held at room temperature. Shorter alkane chains can easily desorb, whereas the strong interaction of *n*-dotriacontane with the surface inhibits desorption at elevated temperatures. The monomers adsorb on the Au (110) surface exclusively along the atomic channels (Figure 1.3a). After subsequent annealing at 440 K, the alkane monomers were bonded end to end, forming long molecular chains within the atomic channels of the Au(110) substrate (Figure 1.3b). The successful polymerization was checked by controlled manipulation experiments with the STM tip, showing that sections of the reacted chains could be pulled out from the substrate grooves (Figure 1.3c) and providing further evidence that the products are covalently bound. It was found that most of the reacted polymers have a length of more than 200 nm. In TPD experiments, the desorption of H_2 could be verified during the thermally activated polymerization pointing to a dehydrogenation polymerization process. This was further confirmed by testing the reaction with 1,4-di(eicosyl)benzene and eicosylbenzene monomers, which both have a phenylene moiety as a marker connecting the alkyl chains (for more details see Ref. [45]). Results from DFT calculations provide a reasonable mechanism for the activation of the monomers, which exclusively takes place at the terminal CH_3 or penultimate CH_2 groups. Furthermore, the DFT results confirm that the orientational constraint of the reconstructed Au(110) surface is a major factor for the reaction to proceed.

1.3
Azide–Alkyne Cycloaddition

Among the many conceivable reactions that have potential to be performed as on-surface processes, azide–alkyne cycloadditions (often referred to as “click” reactions) are interesting candidates due to their strong covalently linked products and their low activation energies [46]. Such reactions are free of by-products and performed as solution-phase processes that have been widely used for the modification of surfaces and materials [47–49] as well as for the preparation of biologically active compounds in pharmaceutical research [50]. The most commonly used “click” reaction is the azide–alkyne 1,3-dipolar cycloaddition [51,52] leading to 1,4- and 1,5-triazoles. Whereas the classical thermal process (Huisgen azide–alkyne [3 + 2]-cycloaddition), which proceeds under

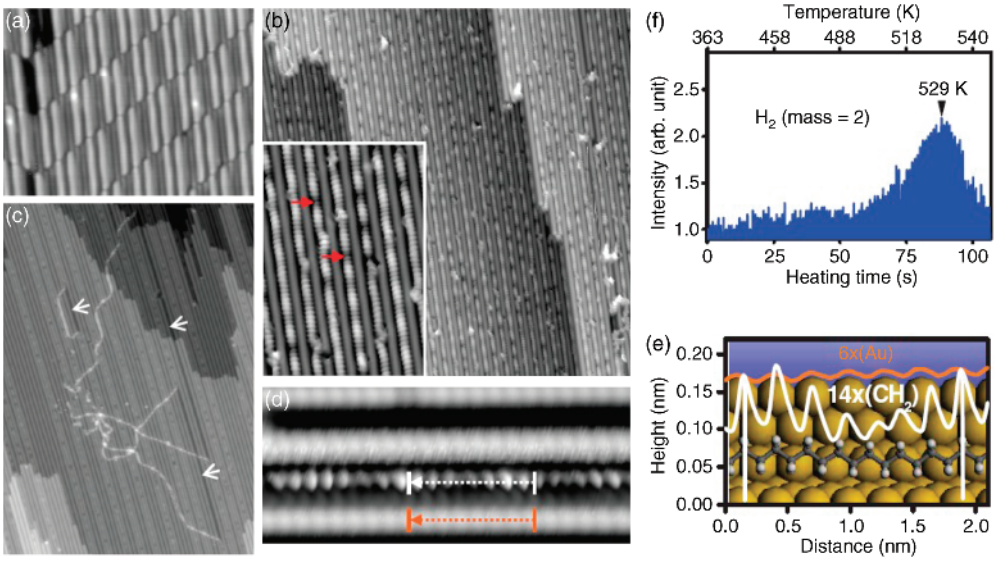

Figure 1.3 Dehydrogenative polymerization of *n*-dotriacontane ($C_{32}H_{66}$). (a) STM image of $C_{32}H_{66}$ monomers on the Au(110)-(1 × 2) surface (20 nm × 15 nm). (b) Parallel polyethylene chains after annealing up to 440 K for 30 min (50 nm × 50 nm; inset: 9 nm × 13 nm). (c) Several polyethylene chains partially released from the grooves by the STM tip manipulations (50 nm × 70 nm). (d) High-resolution STM image of Au atomic rows and polyethylene chain (6 nm × 2.5 nm). (e) Height profiles at the dotted lines in (d). (f) H_2 signal detected by mass spectrometry during the annealing process (heating power: 1.2 A by 10.25 V). (Reprinted with permission from AAAS [45].)

harsh conditions, that is, high temperatures, generally delivers a mixture of the two regioisomers, the use of a copper catalyst provides 1,4-triazoles with high efficiency and regioselectivity under ambient conditions (CuAAC) [51].

Resembling the CuAAC mechanism in solution, a successful cycloaddition of alkynes and azides was recently accomplished on a Cu(111) surface with complete regioselectivity toward the formation of the corresponding 1,4-triazoles [53]. As for the solution-phase process, the high regioselectivity was discussed considering the involvement of a copper acetylide (C−H activation) and bonding of the alkyne group to the Cu(111) surface. However, a strong interaction between the Cu atoms of the surface and the azide moiety causes the degradation of the latter, limiting its reactivity considerably.

In an own recent study, STM experiments and DFT simulations were combined to investigate on-surface cycloaddition reactions of *N*-(4-azidophenyl)-4-ethynylbenzamide (AEB) monomers on a Au(111) surface under UHV conditions [54]. The design of the AEB monomers (Figure 1.4a) is a combination of two phenyl rings connected through an amide linker as backbone, allowing the monomers to be thermally deposited on the surface, where they can lay flat and diffuse, thus increasing the probability of the alkyne and azide groups to meet

with each other and react. The selection of the Au(111) surface as a template is based on an attempt to diminish/prevent the degradation of the azides on the surface, thus enhancing the reactivity.

The deposition of the AEB molecules on the Au(111) surface was carried out by sublimation at a crucible temperature of 85 °C in UHV, while the surface was kept at room temperature. The covered surface usually showed a first layer mixture of reactants mixed with already reacted dimers as well as trimers, surrounded by a disordered molecular phase (Figure 1.4b(i)). Such phase could be ascribed to the azide end group degradation on Au(111) [53]. The quantitative assessment of the yield of the observed cycloaddition revealed that from the total of intact molecules found for four different deposition runs, about 29% reacted to dimers and about 8% to trimers. Around 63% were found as nonreacted monomers. It is interesting to note that the dimerization yield for the cycloaddition on

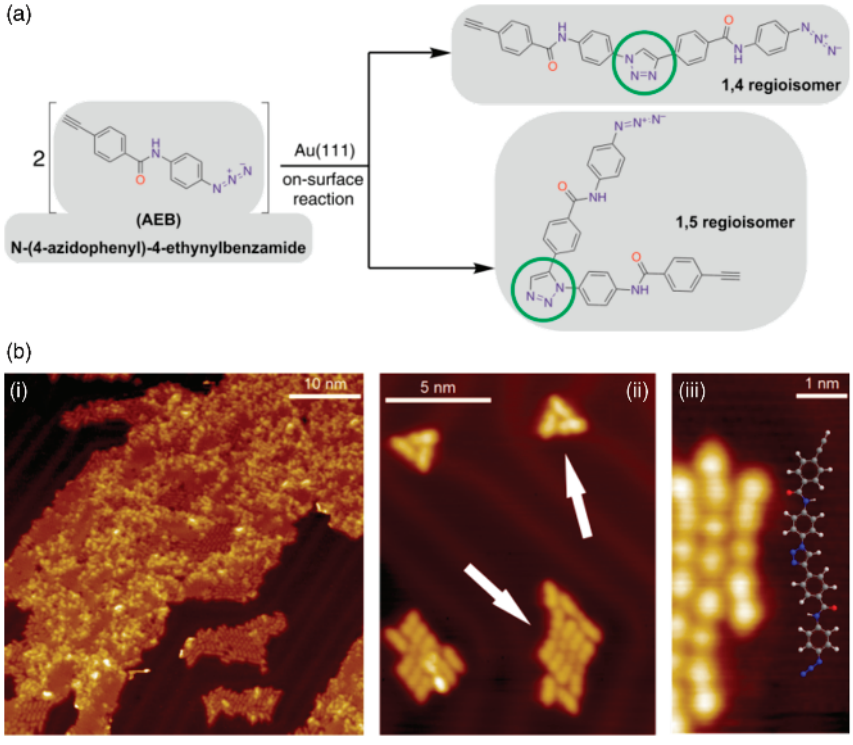

Figure 1.4 (a) Scheme of the proposed on-surface azide–alkyne cycloaddition reaction. Green circles enclose the triazole moieties. (b) STM images of AEB monomer deposition on Au(111) at room temperature. (i) Large coverage deposition (50 nm × 50 nm). (ii) Self-assembly of monomers and dimers (13 nm × 17 nm). (iii) Dimers and trimers formed as a result of the successful azide–alkyne "click" reaction (3.5 nm × 7 nm). *Inset*: Molecular structure of the 1,4-triazole dimer. (Adapted with permission from Ref. [54]. Copyright 2013, American Chemical Society.)

Au(111) is considerably larger than the one observed on Cu(111) [53], which one would expect larger due to the potential catalytic activity of copper. To confirm the covalent linkage of the reactants, controlled manipulations with the STM tip were carried out on the dimers and the trimers. Triazoles are known for their robustness and their high torsional degree of freedom and such features are also displayed by the on-surface coupling products on Au(111).

For a successful on-surface reaction to proceed, two monomers have to diffuse toward each other so that the reactive alkyne and azide functionalities are close enough for successful cycloaddition. Therefore, the self-assembled structure obtained after initial deposition must somehow relate to the reactivity. In our experimental studies, we found the unreacted AEB monomers to be present in three different configurations: (i) nucleation along the step edges, which is in agreement with the alkyne group high affinity for highly reactive sites, such as step edges; (ii) agglomeration adjacent to molecular islands as a result of diffusion of the molecules on the Au(111) surface and self-assembly driven by van der Waals forces; most likely those observed monomers are unreacted remnants, which did not find a counterpart to react with (lower section of Figure 1.4b(ii)); and (iii) self-assembled arrangement of three monomers in a stable triangular shaped island (upper section of Figure 1.4b(ii)). We found this configuration quite frequently (~27% of the monomers that remain intact after the deposition), being the only configuration where exclusively monomers self-assembled independently.

The inset in Figure 1.4b(iii) represents the molecular structure of a 1,4-triazole dimer. This structure matches very well the STM observations, since the alternative 1,5-regioisomer would present a significant tilt (L-shaped structure, see scheme in Figure 1.4a) instead of the observed linear structure. In these experiments, only the formation of the 1,4-regioisomer was observed. DFT calculations showed that the Au substrate (i) lowers the activation energy, which causes the reaction to proceed at room temperature, (ii) does not act as a catalyst but merely as a two-dimensional constraint, and (iii) steers the complete 1,4-regioselectivity of the [3 + 2] on-surface cycloaddition reaction by means of surface-induced steric effects preventing the formation of the 1,5-regioisomer. The fact that the regioselectivity of the azide–alkyne cycloaddition can be controlled by the surface constraint and the reactants' design provides an efficient method to develop well-defined nanostructures at surfaces, without the requirement of a catalyst or additional thermal activation.

1.4 Glaser Coupling

Another interesting coupling mechanism involves the halogen-free reaction of aryl alkynes (Glaser coupling), which was studied at gold and silver surfaces [55]. For initial investigations, the diethynyl-substituted π-system C38, as shown in Figure 1.5a, was studied. Figure 1.5b(i) shows an STM image of the C38 molecule, which forms a self-assembled structure dominated by Van der Waals

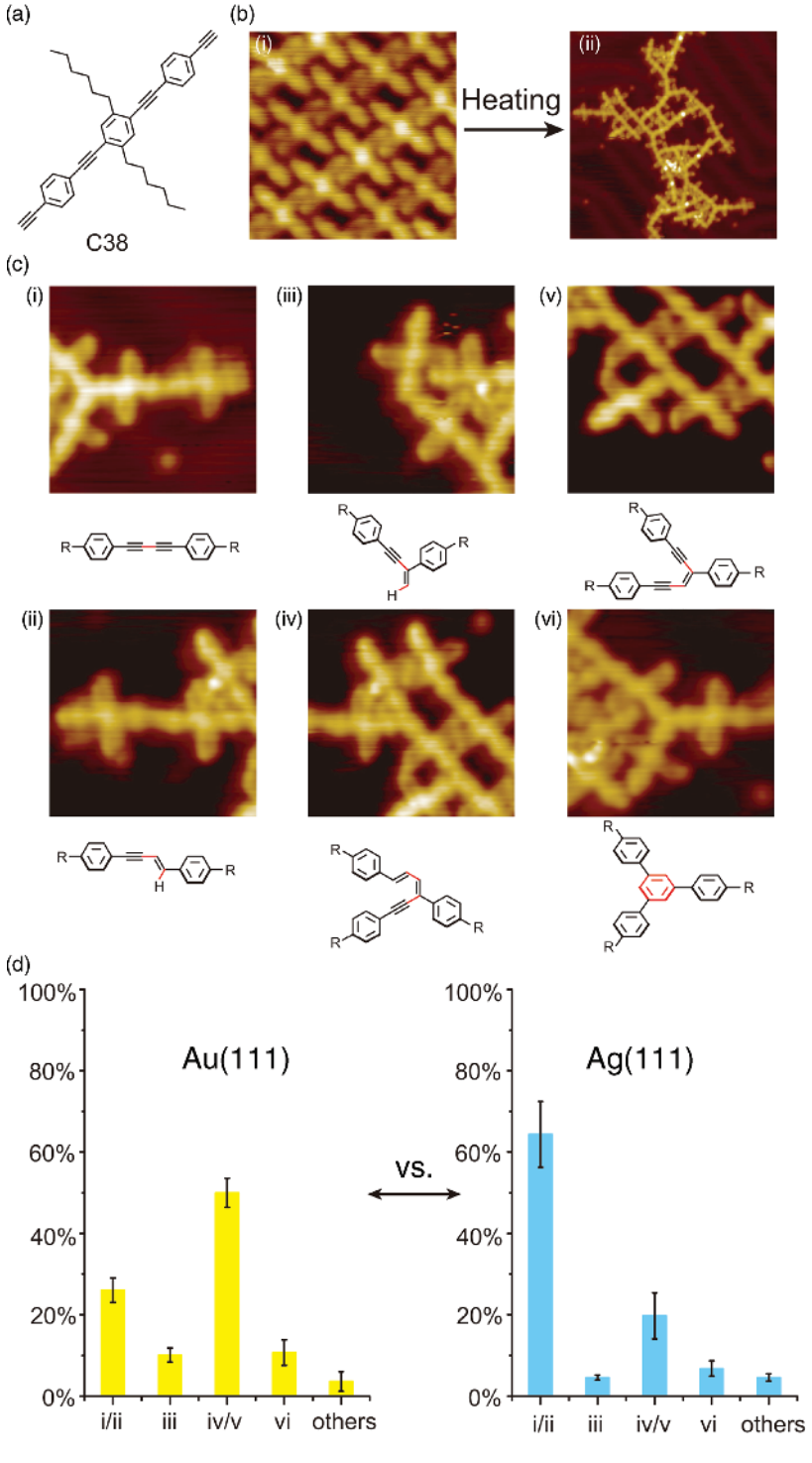
(a)
C38
(b)
(i)
(ii)
Heating
(c)
(i)
(iii)
(v)
(ii)
(iv)
(vi)
R
H
(d)
100%
80%
60%
40%
20%
0%
Au(111)
vs.
Ag(111)
i/ii
iii
iv/v
vi
others

interactions between the C6-alkane chains. After thermal annealing, the C38 molecules form a covalent bound nanostructure via reactions of the alkynes (Figure 1.5b(ii)). However, due to various possible reaction pathways, several side products were identified: Glaser coupling (Figure 1.5c(i)), formal hydroalkynylation of the terminal alkyne functionality either at the α-position or at the β-position (Figure 1.5c(ii) and (iii)), dieyne products (Figure 1.5c(iv)), enediyne moiety (Figure 1.5c(v)), and diyne polycyclotrimerization (Figure 1.5c(vi)). To further study the catalytic role of the metal surface, the relative frequency of occurrence of the reaction pathways (i)–(vi) was determined on the Au(111) and Ag(111) surfaces. As in some cases the reactions (i) and (ii), as well as (iv) and (v), were undistinguishable, they were combined in this analysis. However, it is important to note that the Glaser reaction (i) is the main reaction type within the (i)/(ii) pair of the statistical analysis. It was found that the reaction pathways (i)/(ii) and (iv)/(v) occurred with frequencies of (26 ± 3) and (50 ± 3.6)% on the Au(111) surface, while frequencies of (64.3 ± 8.1) and (19.7 ± 5.7)% were found on the Ag(111) surface, respectively. Thus, Glaser coupling seems to be more efficient on Ag(111) than on Au(111) surfaces, while the side reactions (iv)/(v) reverse.

To further improve the selectivity toward Glaser coupling, dimers of 1,4-diethynylbenzene having no alkane chains on its side (C20, Figure 1.6a(i)) were tested as alternative reactants. Deposited on the Au(111) surface, they formed ordered (Figure 1.6a(ii)) as well as disordered self-assembled structures [55]. After annealing, branched covalent bound nanostructures can be observed (Figure 1.6a(iii)). In a similar statistical analysis as for the C38 case, Glaser coupling events occurred at a frequency of (43.3 ± 4.3)% on the Au(111) surface. The selectivity toward this reaction type could be further improved by performing the experiment on the Ag(111) surface, where a frequency of (67 ± 3.8)% could be achieved. At the same time, the side reactions (iv)/(v) were slightly reduced to (40.8 ± 4.1)% on the Au(111) surface and (21.6 ± 3.6)% on the Ag(111) surface.

By further optimization of the precursor molecules, the side reactions of alkynes could be completely suppressed. Figure 1.6b(i) shows the structure of the resulting C22 molecule with an *ortho*-substituent next to the alkyne functionality, which suppresses side reactions due to steric reasons. As shown in Figure 1.6b (ii), STM images of the self-assembled C22 molecules on Au(111) match its chemical structure very well. After reaction, C22 molecules were mainly connected one by one through Glaser coupling (Figure 1.6b(iii)). The length of the

Figure 1.5 Glaser coupling of the C38 molecule. (a) Molecular chemical structure. (b) High-resolution STM image of C38 precursors at a Au(111) surface (i: 6 nm × 6 nm), as well as high-resolution image of C38 oligomers after thermal annealing at 123–140 °C (ii: 25 nm × 25 nm). (c) Rationalization of the different observed covalent bonding types in on-surface oligomerization by STM images (all with 6 nm × 6 nm) and the corresponding chemical structures. (d) Corresponding statistical analysis for the distribution of the observed products on Au(111) and Ag(111) surfaces, which clearly prove that the Ag(111) surface works more efficiently toward the Glaser coupling. (Redrawn with permission from Wiley-VCH Verlag GmbH [55].)

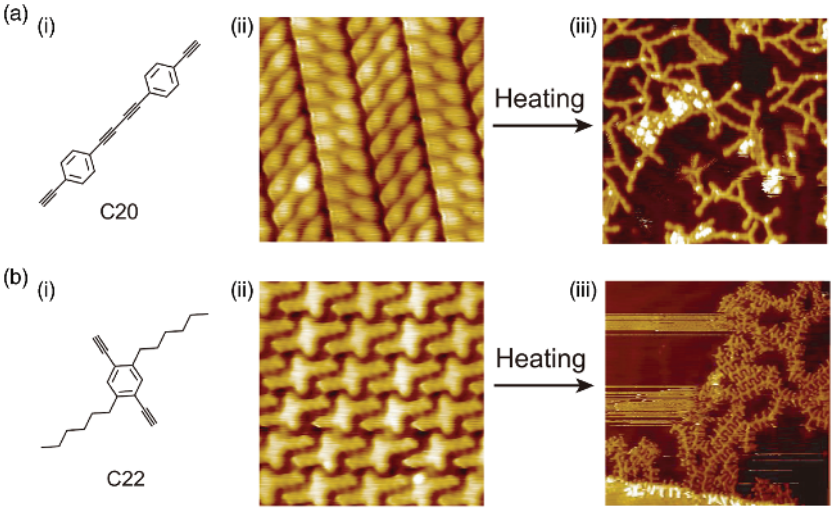

(c)

Au(111) vs. Ag(111)

Reaction / Molecules	i/ii	iii	iv/v	vi	others
C38	26±3 %	10.1±1.7 %	50±3.6 %	10.7±3.1 %	3.6±2.4 %
	64.3±8.1 %	4.6±0.6 %	19.7±5.7 %	6.8±1.9 %	4.6±0.9 %
C20	43.3±4.3%	2.3±2.3%	40.8±4.1%	7.1±3.3 %	6.5±1.4 %
	67±3.8%	4.4±0.7%	21.6±3.6%	2.4±0.7 %	4.7±1.7 %
C22	92.1±5.2 %	2.6±0.9 %	0	2.2±2.7%	3.1±1.1%
	96.4±1.7 %	0.8±0.4 %	0	1.7±0.8%	1.1±1.1%

Figure 1.6 Glaser coupling of C20 and C22 molecules. (a) Chemical structure of the C20 molecule (i) and its high-resolution STM images before (ii: 6 nm × 6 nm) and after (iii: 25 nm × 25 nm) the Glaser coupling reaction on the Au(111) substrate. (b) Chemical structure of the C22 molecule (i) and its high-resolution STM images before (ii: 6 nm × 6 nm) and after (ii: 25 nm × 25 nm) reaction on the Au(111) substrate. (c) Summary of the statistical analysis for the distribution of the observed products on the different substrates allowing the comparison of the catalytic abilities of Au(111) and Ag(111) surfaces toward Glaser coupling, side cross-coupling, and the influences of chemical structures from C38 to C20 and C22. ((a) Adapted with permission from Ref. [56]. Copyright 2013, American Chemical Society. (b) Redrawn with permission from Wiley-VCH Verlag GmbH [55].)

polymers could be increased up to 59 monomers when Ag(111) was used as a substrate. The statistical analysis revealed that the Glaser coupling was optimized up to $(92.1 \pm 5.1)\%$ on Au(111) and $(96.4 \pm 1.7)\%$ on Ag(111). At the same time, the side reactions (iv)/(v) were completely suppressed.

Figure 1.6c shows a summary of the statistical frequencies for the different tested reactants C38, C20, and C22. As indicated by the yellow arrow, the *ortho*-substituent next to the alkyne works very efficiently toward chemical selectivity of Glaser coupling in alkyne reactions. Another important point is that the Ag (111) surface has a stronger catalytic effect toward Glaser coupling than the Au (111) surface, where the latter leads to more side reactions. To understand the different catalytic effects of on-surface Glaser coupling on metal surfaces, DFT simulations were conducted [56]. The results suggest a model with two possible reaction pathways: C−C coupling via direct C−H activation and C−C coupling via alkynyl activation by π-complex formation. On both Au and Ag surfaces, the alkyne direct C−H activation was found to be a high-energy pathway (1.64 and 1.85 eV on Au and Ag, respectively), which is very unlikely to occur in experiments. The alternative low-energy route (0.79 and 0.9 eV on Au and Ag, respectively) comprises interaction of the alkyne functionality with the surface and direct C−C bond formation as the rate-determining step.

In a subsequent study on the (111) surfaces of Ag, Au, and Cu, photoinduced effects on the Glaser coupling were investigated by exposing self-assembled monolayers of the C22 molecule to UV irradiation [57]. As shown in Figure 1.7a, the formation of aryl alkyne dimers at the Ag(111) surface could be induced after UV irradiation for 67 h at a wavelength of 375 nm. This photochemical aryl alkyne dimerization occurred also on Cu(111), but with a significantly reduced efficiency compared with Ag(111). On the gold surface, no photoinduced effects could be observed at all, emphasizing the catalytic role of the substrate also for the photoinduced approach of the Glaser coupling. Short aryl alkyne oligomers such as trimers and tetramers could be observed on the Ag(111) surface as shown in Figure 1.7b. The statistical analysis of the oligomer length distribution shows that the main products of photochemical reaction of the C22 molecules are the dimers with an abundance of $(87.4 \pm 2.1)\%$, which significantly differs from the products of the thermally induced C22 reactions on Ag(111). In comparison with the thermal process, the major advantage of the photochemical on-surface reaction at room temperature is that the self-assembly of the reactants after initial deposition may be restored, allowing spatiotemporal control of the C−C bond formation. The DFT simulations indicate why the Ag surface is more efficient than Au. This is because the gold surface interacts stronger with the alkynyl groups resulting in a reduced mobility of the molecules on the substrate and a longer trapping of C−C coupled intermediates to branching reactions.

1.5 Decarboxylative Polymerization of Acids

The metal-catalyzed polymerization of 2,6-naphthalenedicarboxylic acid (NDCA) is another important recent achievement in the research filed [58]. The C−C coupling of NDCAs was found to occur via a three-step process, which is visualized in the scheme in Figure 1.8a: step 1 is a dehydrogenation process to

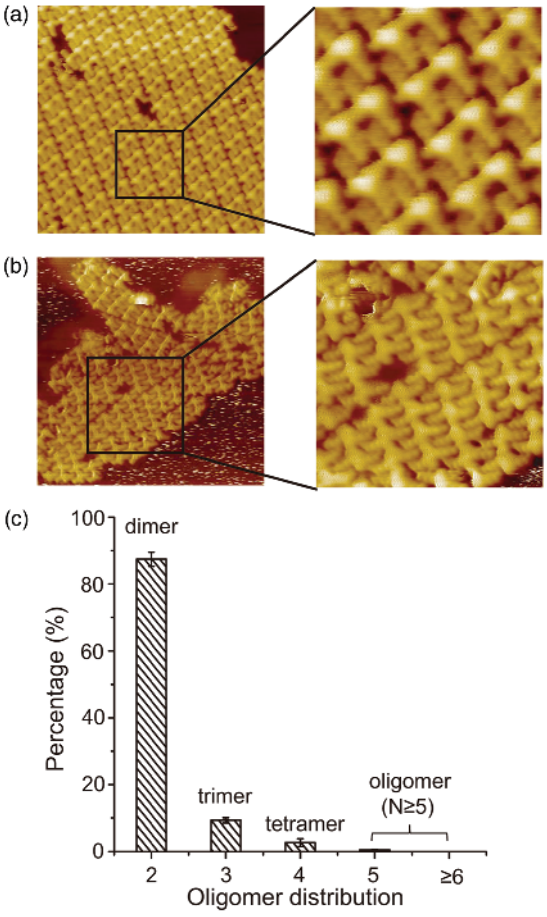

Figure 1.7 Photochemical Glaser coupling of the C22 molecule after UV irradiation (67 h) on Ag(111). (a) STM image of C22 dimers (17 nm × 17 nm), with a high-resolution image shown in the inset (5 nm × 5 nm). (b) STM image of short C22 oligomers (20 nm × 20 nm), with an inset image (8.4 nm × 8.4 nm). (c) The corresponding statistical analysis for the oligomer distribution. (Adapted with permission from Ref. [57]. Copyright 2014, American Chemical Society.)

provide the corresponding metal carboxylate; in step 2, a decarboxylative process leads to the formation of polymeric bisnaphthyl-Cu as an intermediate species; and step 3 finally leads to C−C coupling forming poly-2,6-naphthalnene chains via decarboxylation. First of all, it was found that this reaction seems generally not to proceed on the Au(111) surface. Switching to the Ag(111) surface, the interaction of the carboxyl group with the substrate could be increased and covalent coupling of NDCAs occurred after thermal annealing to 156 °C. However, due to the desorption of NDCA during annealing, the efficiency toward poly-bisnaphthyl-Ag intermediates as well as the oligo-2,6-naphthalene was

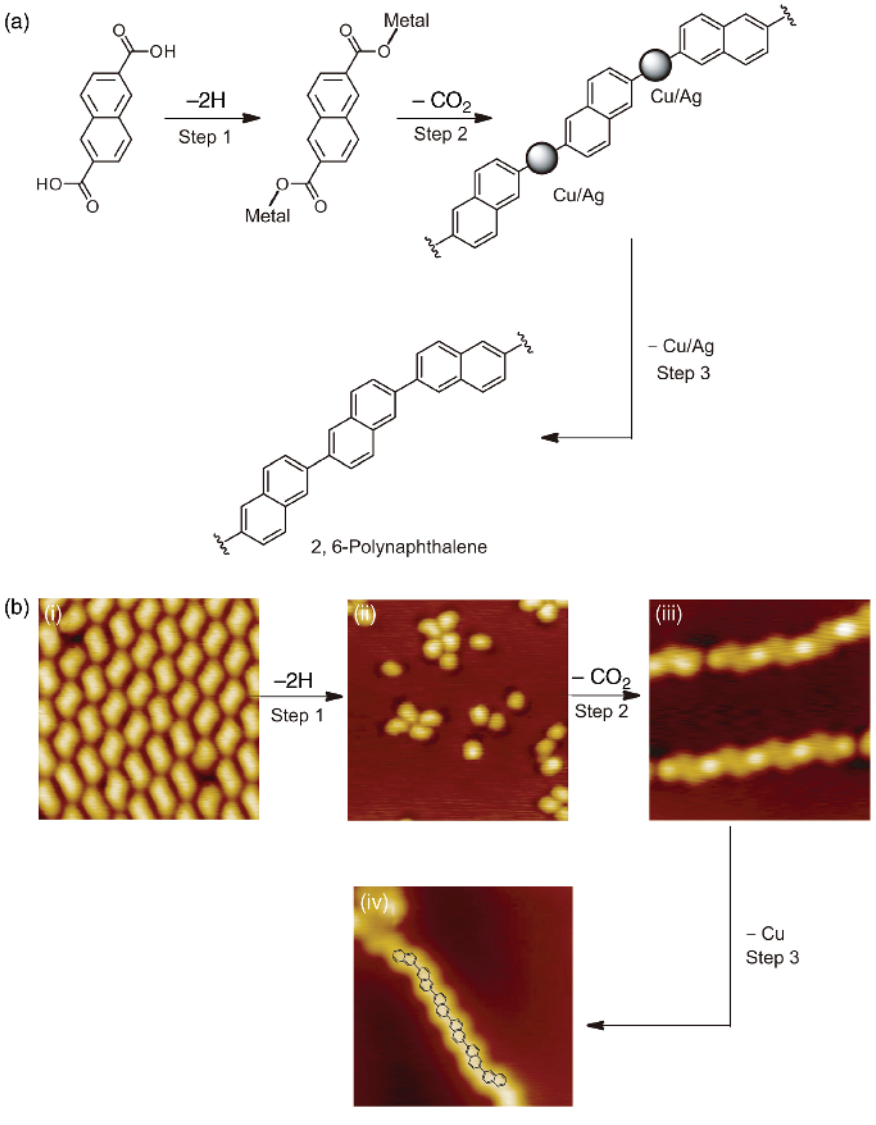

Figure 1.8 Metal-catalyzed on-surface polymerization of NDCA. (a) Schematic illustration of the reaction pathway. (b) STM images for the polymerization of NDCA on Cu(111) from unreacted precursor molecules (i: 6 nm × 6 nm), to their dehydrogenated state (ii: 10 nm × 10 nm), via the bisnaphthyl-Cu intermediates (iii: 4.24 nm × 4.24 nm), and finally to poly-2,6-naphthalene (iv: 4.2 nm × 4.2 nm). (Adapted with permission from Ref. [58]. Copyright 2014, American Chemical Society.)

rather low. Therefore, Cu(111) was tested as substrate for the reaction, as it shows the strongest interaction with carboxyl groups compared with the Au(111) or Ag(111) surfaces. Expectedly, a hydrogen-bonded self-assembly structure (one of the different phases is shown in Figure 1.8b(i)), dehydrogenated product (Figure 1.8b(ii)), bisnaphthyl-Cu species (Figure 1.8b(iii)), and final polynaphthalenes (Figure 1.8b(iv)) were obtained with high efficiency. Moreover, the differences of Cu(111), Cu(100), and Cu(110) surfaces were compared toward such decarboxylative polymerization. Surprisingly, the following reactivity order was observed: Cu(111) > Cu(100) > Cu(110), which likely relates to the ability of metal atoms being pulled out of the surface. The experiments also revealed that the organometallic polymers (bisnaphthalene-Cu species) on the Cu(100) surface were grown only in [001] and [010] directions, while organometallic polymers on the Cu(111) surface grow in [110], [011], and [101] directions. This substrate dependence indicates that the metal atoms part of the organometallic polymers should have a specific interaction with the metal surfaces.

1.6 Conclusions

An interesting feature of on-surface chemical reactions is the possibility of targeted conjugation in more than one direction on a substrate, extending 1D polymerization to the growth of 2D organic networks. Thereby, on-surface reactions performed under UHV conditions benefit from the lack of solvents required, which allows us to gain insight into chemical processes under well-defined conditions. The recent achievements in this research field allow to identify some important prerequisites for a successful covalent coupling, which are summarized in the following.

An important aspect is the flat adsorption geometry of the reactants, where the adsorption strength is crucial to avoid desorption when the system is supplied with additional energy by thermal annealing and/or light illumination. In particular, it has been observed to impact directly the ordering of the products after the on-surface coupling [55,59,60]. Too strongly adsorbed molecules might inhibit a reaction by reduced diffusion, which is vital for the reactive moieties to meet in the desired geometry on a surface. Therefore, reduced diffusion can lead to poor reactivity and stereocontrol [55,59,60]. For experiments under UHV conditions, the design of the reactants should enable a straightforward deposition, which in most cases is done by thermal sublimation. Potential issues could be the decomposition of the molecules or reactive end groups due to the elevated sublimation temperatures in the crucible. For the proper design of the reactants, steric effects on the surface should be considered, providing further control on the reaction mechanism, for example, in view of regioselectivity of the anticipated bond formation. Another important aspect is the choice of the substrate. As shown earlier, a surface can act as both a two-dimensional spatial constraint [54] and an active catalytic agent in a specific reaction mechanism [28,45]. Therefore, a

simple transfer of reaction mechanisms from solution-phase chemistry to on-surface reactions is not straightforward. Furthermore, surface orientation, reconstructions, or well-oriented stepped surfaces can help to provide directional alignment of the products [23,28,29,45]. Finally, reaction by-products are usually detrimental for the properties of a highly defined nanomaterial and can hinder the studied process or even suppress it [26].

Given the remarkable achievements of the last few years in the field of on-surface reactions with organic molecules, a promising approach for the development of novel nanomaterials with tailored optoelectronic properties and potential applications in devices emerged. The current major challenges are to determine the critical parameters to control reaction pathways and material properties in the two-dimensional environment of a surface. However, future work should also focus on extending the existing tool kit of on-surface chemistry by finding additional reaction pathways.

Acknowledgments

The authors acknowledge support by the Deutsche Forschungsgemeinschaft (DFG) through the Collaborative Research Center SFB 858, project B2, and TRR 61, projects B3 and B7.

References

1 Barth, J.V. (2007) Molecular architectonic on metal surfaces. *Annu. Rev. Phys. Chem.*, **58**, 375–407.
2 Champness, N.R. (2012) Surface chemistry making the right connections. *Nat. Chem.*, **4** (3), 149–150.
3 Gourdon, A. (2008) On-surface covalent coupling in ultrahigh vacuum. *Angew. Chem., Int. Ed.*, **47** (37), 6950–6953.
4 Mendez, J., Lopez, M.F., and Martin-Gago, J.A. (2011) On-surface synthesis of cyclic organic molecules. *Chem. Soc. Rev.*, **40** (9), 4578–4590.
5 Zhang, X.M., Zeng, Q.D., and Wang, C. (2013) On-surface single molecule synthesis chemistry: a promising bottom-up approach towards functional surfaces. *Nanoscale*, **5** (18), 8269–8287.
6 Franc, G. and Gourdon, A. (2011) Covalent networks through on-surface chemistry in ultra-high vacuum: state-of-the-art and recent developments. *Phys. Chem. Chem. Phys.*, **13** (32), 14283–14292.
7 Sakamoto, J., van Heijst, J., Lukin, O., and Schluter, A.D. (2009) Two-dimensional polymers: just a dream of synthetic chemists? *Angew. Chem., Int. Ed.*, **48** (6), 1030–1069.
8 Perepichka, D.F. and Rosei, F. (2009) Chemistry. Extending polymer conjugation into the second dimension. *Supramol. Sci.*, **323** (5911), 216–217.
9 de Oteyza, D.G., Gorman, P., Chen, Y.C., Wickenburg, S., Riss, A., Mowbray, D.J., Etkin, G., Pedramrazi, Z., Tsai, H.Z., Rubio, A., Crommie, M.F., and Fischer, F.R. (2013) Direct imaging of covalent bond structure in single-molecule chemical reactions. *Supramol. Sci.*, **340** (6139), 1434–1437.
10 Swart, I., Gross, L., and Liljeroth, P. (2011) Single-molecule chemistry and physics explored by low-temperature scanning probe microscopy. *Chem. Commun.*, **47** (32), 9011–9023.
11 Repp, J., Meyer, G., Paavilainen, S., Olsson, F.E., and Persson, M. (2006) Imaging bond

formation between a gold atom and pentacene on an insulating surface. *Supramol. Sci.*, **312** (5777), 1196–1199.

12 Okawa, Y., Akai-Kasaya, M., Kuwahara, Y., Mandal, S.K., and Aono, M. (2012) Controlled chain polymerisation and chemical soldering for single-molecule electronics. *Nanoscale*, **4** (10), 3013–3028.

13 Okawa, Y., Mandal, S.K., Hu, C., Tateyama, Y., Goedecker, S., Tsukamoto, S., Hasegawa, T., Gimzewski, J.K., and Aono, M. (2011) Chemical wiring and soldering toward all-molecule electronic circuitry. *J. Am. Chem. Soc.*, **133** (21), 8227–8233.

14 Hla, S.W., Bartels, L., Meyer, G., and Rieder, K.H. (2000) Inducing all steps of a chemical reaction with the scanning tunneling microscope tip: towards single molecule engineering. *Phys. Rev. Lett.*, **85** (13), 2777–2780.

15 Zhao, A., Tan, S.J., Li, B., Wang, B., Yang, J.L., and Hou, J.G. (2013) STM tip-assisted single molecule chemistry. *Phys. Chem. Chem. Phys.*, **15** (30), 12428–12441.

16 Custance, O., Perez, R., and Morita, S. (2009) Atomic force microscopy as a tool for atom manipulation. *Nat. Nanotechnol.*, **4** (12), 803–810.

17 Kittelmann, M., Nimmrich, M., Lindner, R., Gourdon, A., and Kuhnle, A. (2013) Sequential and site-specific on-surface synthesis on a bulk insulator. *ACS Nano*, **7** (6), 5614–5620.

18 Grill, L., Dyer, M., Lafferentz, L., Persson, M., Peters, M.V., and Hecht, S. (2007) Nano-architectures by covalent assembly of molecular building blocks. *Nat. Nanotechnol.*, **2** (11), 687–691.

19 Lafferentz, L., Eberhardt, V., Dri, C., Africh, C., Comelli, G., Esch, F., Hecht, S., and Grill, L. (2012) Controlling on-surface polymerization by hierarchical and substrate-directed growth. *Nat. Chem.*, **4** (3), 215–220.

20 Saywell, A., Schwarz, J., Hecht, S., and Grill, L. (2012) Polymerization on stepped surfaces: alignment of polymers and identification of catalytic sites. *Angew. Chem., Int. Ed.*, **51** (21), 5096–5100.

21 Lafferentz, L., Ample, F., Yu, H., Hecht, S., Joachim, C., and Grill, L. (2009) Conductance of a single conjugated polymer as a continuous function of its length. *Supramol. Sci.*, **323** (5918), 1193–1197.

22 Gutzler, R., Walch, H., Eder, G., Kloft, S., Heckl, W.M., and Lackinger, M. (2009) Surface mediated synthesis of 2D covalent organic frameworks: 1,3,5-tris(4-bromophenyl)benzene on graphite(001), Cu(111), and Ag(110). *Chem. Commun.*, **29**, 4456–4458.

23 Cai, J.M., Ruffieux, P., Jaafar, R., Bieri, M., Braun, T., Blankenburg, S., Muoth, M., Seitsonen, A.P., Saleh, M., Feng, X.L., Mullen, K., and Fasel, R. (2010) Atomically precise bottom-up fabrication of graphene nanoribbons. *Nature*, **466** (7305), 470–473.

24 Eichhorn, J., Strunskus, T., Rastgoo-Lahrood, A., Samanta, D., Schmittel, M., and Lackinger, M. (2014) On-surface Ullmann polymerization via intermediate organometallic networks on Ag(111). *Chem. Commun. (Camb.)*, **50** (57), 7680–7682.

25 Eder, G., Smith, E.F., Cebula, I., Heckl, W. M., Beton, P.H., and Lackinger, M. (2013) Solution preparation of two-dimensional covalently linked networks by polymerization of 1,3,5-tri(4-iodophenyl) benzene on Au(111). *ACS Nano*, **7** (4), 3014–3021.

26 Schlogl, S., Heckl, W.M., and Lackinger, M. (2012) On-surface radical addition of triply iodinated monomers on Au(111): the influence of monomer size and thermal post-processing. *Surf. Sci.*, **606** (13–14), 999–1004.

27 Lipton-Duffin, J.A., Ivasenko, O., Perepichka, D.F., and Rosei, F. (2009) Synthesis of polyphenylene molecular wires by surface-confined polymerization. *Small*, **5** (5), 592–597.

28 Zhang, H., Franke, J.H., Zhong, D., Li, Y., Timmer, A., Díaz Arado, O., Mönig, H., Wang, H., Chi, L., Wang, Z., Mullen, K., and Fuchs, H. (2014) Surface supported gold–organic hybrids: on-surface synthesis and surface directed orientation. *Small*, **10** (7), 1361–1368.

29 Linden, S., Zhong, D., Timmer, A., Aghdassi, N., Franke, J.H., Zhang, H., Feng, X., Mullen, K., Fuchs, H., Chi, L., and Zacharias, H. (2012) Electronic structure of spatially aligned graphene

nanoribbons on Au(788). *Phys. Rev. Lett.*, **108** (21), 216801.

30 Nazin, G.V., Qiu, X.H., and Ho, W. (2003) Visualization and spectroscopy of a metal–molecule–metal bridge. *Supramol. Sci.*, **302** (5642), 77–81.

31 Koudia, M. and Abel, M. (2014) Step-by-step on-surface synthesis: from manganese phthalocyanines to their polymeric form. *Chem. Commun.*, **50**, 8565–8567.

32 Zhang, H.-M., Zhao, W., Xie, Z.-X., Long, L.-S., Mao, B.-W., Xu, X., and Zheng, L.-S. (2007) One step fabrication of metal–organic coordination monolayers on Au(111) surfaces. *J. Phys. Chem. C*, **111** (21), 7570–7573.

33 Dienstmaier, J.F., Medina, D.D., Dogru, M., Knochel, P., Bein, T., Heckl, W.M., and Lackinger, M. (2012) Isoreticular two-dimensional covalent organic frameworks synthesized by on-surface condensation of diboronic acids. *ACS Nano*, **6** (8), 7234–7242.

34 Xu, L.R., Zhou, X., Yu, Y.X., Tian, W.Q., Ma, J., and Lei, S.B. (2013) Surface-confined crystalline two-dimensional covalent organic frameworks via on-surface Schiff-base coupling. *ACS Nano*, **7** (9), 8066–8073.

35 Treier, M., Fasel, R., Champness, N.R., Argent, S., and Richardson, N.V. (2009) Molecular imaging of polyimide formation. *Phys. Chem. Chem. Phys.*, **11** (8), 1209–1214.

36 Treier, M., Richardson, N.V., and Fasel, R. (2008) Fabrication of surface-supported low-dimensional polyimide networks. *J. Am. Chem. Soc.*, **130** (43), 14054–14055.

37 Weigelt, S., Busse, C., Bombis, C., Knudsen, M.M., Gothelf, K.V., Laegsgaard, E., Besenbacher, F., and Linderoth, T.R. (2008) Surface synthesis of 2D branched polymer nanostructures. *Angew. Chem., Int. Ed.*, **47** (23), 4406–4410.

38 Weigelt, S., Busse, C., Bombis, C., Knudsen, M.M., Gothelf, K.V., Strunskus, T., Woll, C., Dahlbom, M., Hammer, B., Laegsgaard, E., Besenbacher, F., and Linderoth, T.R. (2007) Covalent interlinking of an aldehyde and an amine on a Au(111) surface in ultrahigh vacuum. *Angew. Chem., Int. Ed.*, **46** (48), 9227–9230.

39 Marele, A.C., Mas-Balleste, R., Terracciano, L., Rodriguez-Fernandez, J., Berlanga, I., Alexandre, S.S., Otero, R., Gallego, J.M., Zamora, F., and Gomez-Rodriguez, J.M. (2012) Formation of a surface covalent organic framework based on polyester condensation. *Chem. Commun.*, **48** (54), 6779–6781.

40 Schmitz, C.H., Ikonomov, J., and Sokolowski, M. (2011) Two-dimensional polyamide networks with a broad pore size distribution on the Ag(111) surface. *J. Phys. Chem. C*, **115** (15), 7270–7278.

41 Faury, T., Dumur, F., Clair, S., Abel, M., Porte, L., and Gigmes, D. (2013) Side functionalization of diboronic acid precursors for covalent organic frameworks. *CrystEngComm*, **15** (11), 2067–2075.

42 Zwaneveld, N.A.A., Pawlak, R., Abel, M., Catalin, D., Gigmes, D., Bertin, D., and Porte, L. (2008) Organized formation of 2D extended covalent organic frameworks at surfaces. *J. Am. Chem. Soc.*, **130** (21), 6678–6679.

43 Clair, S., Abel, M., and Porte, L. (2014) Growth of boronic acid based two-dimensional covalent networks on a metal surface in ultrahigh vacuum. *Chem. Commun.*, **50**, 9627–9635.

44 Faury, T., Clair, S., Abel, M., Dumur, F., Gigmes, D., and Porte, L. (2012) Sequential linking to control growth of a surface covalent organic framework. *J. Phys. Chem. C*, **116** (7), 4819–4823.

45 Zhong, D.Y., Franke, J.H., Podiyanachari, S.K., Blomker, T., Zhang, H.M., Kehr, G., Erker, G., Fuchs, H., and Chi, L.F. (2011) Linear alkane polymerization on a gold surface. *Supramol. Sci.*, **334** (6053), 213–216.

46 Kolb, H.C., Finn, M.G., and Sharpless, K.B. (2001) Click chemistry: diverse chemical function from a few good reactions. *Angew. Chem., Int. Ed.*, **40** (11), 2004–2021.

47 Binder, W.H. and Sachsenhofer, R. (2007) 'Click' chemistry in polymer and materials science. *Macromol. Rapid Commun.*, **28** (1), 15–54.

48 Li, Y. and Cai, C.Z. (2011) Click chemistry-based functionalization on non-oxidized silicon substrates. *Chem. Asian J.*, **6** (10), 2592–2605.

49 Yao, K.J. and Tang, C.B. (2013) Controlled polymerization of next-generation renewable monomers and beyond. *Macromolecules*, **46** (5), 1689–1712.

50 Kolb, H.C. and Sharpless, K.B. (2003) The growing impact of click chemistry on drug discovery. *Drug Discov. Today*, **8** (24), 1128–1137.

51 Rostovtsev, V.V., Green, L.G., Fokin, V.V., and Sharpless, K.B. (2002) A stepwise Huisgen cycloaddition process: copper(I)-catalyzed regioselective "ligation" of azides and terminal alkynes. *Angew. Chem., Int. Ed.*, **41** (14), 2596–2599.

52 Tornoe, C.W., Christensen, C., and Meldal, M. (2002) Peptidotriazoles on solid phase: [1,2,3]-triazoles by regiospecific copper(I)-catalyzed 1,3-dipolar cycloadditions of terminal alkynes to azides. *J. Org. Chem.*, **67** (9), 3057–3064.

53 Bebensee, F., Bombis, C., Vadapoo, S.R., Cramer, J.R., Besenbacher, F., Gothelf, K. V., and Linderoth, T.R. (2013) On-surface azide–alkyne cycloaddition on Cu(111): does it "click" in ultrahigh vacuum? *J. Am. Chem. Soc.*, **135** (6), 2136–2139.

54 Díaz Arado, O., Mönig, H., Wagner, H., Franke, J.H., Langewisch, G., Held, P.A., Studer, A., and Fuchs, H. (2013) On-surface azide–alkyne cycloaddition on Au (111). *ACS Nano*, **7** (10), 8509–8515.

55 Gao, H.Y., Wagner, H., Zhong, D., Franke, J.H., Studer, A., and Fuchs, H. (2013) Glaser coupling at metal surfaces. *Angew. Chem., Int. Ed.*, **52** (14), 4024–4028.

56 Gao, H.Y., Franke, J.H., Wagner, H., Zhong, D.Y., Held, P.A., Studer, A., and Fuchs, H. (2013) Effect of metal surfaces in on-surface Glaser coupling. *J. Phys. Chem. C*, **117** (36), 18595–18602.

57 Gao, H.Y., Zhong, D.Y., Mönig, H., Wagner, H., Held, P.A., Timmer, A., Studer, A., and Fuchs, H. (2014) Photochemical Glaser coupling at metal surfaces. *J. Phys. Chem. C*, **118** (12), 6272–6277.

58 Gao, H.-Y., Held, P.A., Knor, M., Mück-Lichtenfeld, C., Neugebauer, J., Studer, A., and Fuchs, H. (2014) Decarboxylative polymerization of 2,6-naphthalenedicarboxylic acid at surfaces. *J. Am. Chem. Soc.*, **136** (27), 9658–9663.

59 Pinardi, A.L., Otero-Irurueta, G., Palacio, I., Martinez, J.I., Sanchez-Sanchez, C., Tello, M., Rogero, C., Cossaro, A., Preobrajenski, A., Gomez-Lor, B., Jancarik, A., Stara, I.G., Stary, I., Lopez, M.F., Mendez, J., and Martin-Gago, J.A. (2013) Tailored formation of N-doped nanoarchitectures by diffusion-controlled on-surface (cyclo)dehydrogenation of heteroaromatics. *ACS Nano*, **7** (4), 3676–3684.

60 Bieri, M., Nguyen, M.T., Groning, O., Cai, J., Treier, M., Ait-Mansour, K., Ruffieux, P., Pignedoli, C.A., Passerone, D., Kastler, M., Mullen, K., and Fasel, R. (2010) Two-dimensional polymer formation on surfaces: insight into the roles of precursor mobility and reactivity. *J. Am. Chem. Soc.*, **132** (46), 16669–16676.